Desalination and Water Treatment
www.deswater.com

doi: 10.5004/dwt.2021.26852

216 (2021) 401–411
March

Adsorption of Remazol Brilliant Violet 5R dye from aqueous solution onto melunak and rubberwood sawdust based activated carbon: interaction mechanism, isotherm, kinetic and thermodynamic properties

Azduwin Khasri[a,*], Mohd Ridzuan Mohd Jamir[b], Anis Atikah Ahmad[a], Mohd Azmier Ahmad[c]

[a]*Faculty of Chemical Engineering Technology, Universiti Malaysia Perlis (UniMAP), Perlis, Malaysia, emails: azduwin@unimap.edu.my (A. Khasri), anisatikah@unimap.edu.my (A.A. Ahmad)*
[b]*Faculty of Mechanical Engineering Technology, Universiti Malaysia Perlis (UniMAP), Perlis, Malaysia, email: ridzuanjamir@unimap.edu.my*
[c]*School of Chemical Engineering, Engineering Campus, Universiti Sains Malaysia, 14300 Nibong Tebal, Pulau Pinang, Malaysia, email: chazmier@usm.my*

Received 3 July 2020; Accepted 27 November 2020

ABSTRACT

In this work, melunak and rubberwood-based activated carbon (MAC and RAC) were prepared via microwave induced KOH activation for Remazol Brilliant Violet 5R (RBV5R) dye removal from aqueous solution. Batch adsorption experiments were carried out to evaluate the influence of pH, initial dye concentration, and contact time. The textural characterization shows high BET surface area of 914.0 and 796.0 m^2/g for MAC and RAC, respectively, which indicate that they are comprised of a micro-mesoporous structure. Langmuir isotherms provided the best model for MAC and RAC adsorption data. The adsorption capacities of RBV5R onto MAC and RAC estimated by the Langmuir model were 238.33 and 204.08 mg/g, respectively. The pseudo-first-order, pseudo-second-order, and Elovich model equations were used to analyse the kinetic data of the adsorption process, and both data fitted well with the pseudo-second-order kinetic model. Film diffusion was the rate-limiting step controlling adsorption based on intraparticle diffusion and the Boyd plot. The adsorption mechanisms involved are pore filling, hydrogen bonding, n–π interactions, and π–π interactions. The thermodynamic parameters confirmed that the adsorption was spontaneous, feasible, and endothermic. Furthermore, a mechanism including physisorption and chemisorption of RBV5R on MAC and RAC has been proposed. The desorption study predicts excellent regenerative efficacy of both MAC and RAC for up to four cycles.

Keywords: Activated carbon; Microwave activation; Melunak sawdust; Rubberwood sawdust; Remazol Brilliant Violet 5R; Interaction mechanism

1. Introduction

In view of their colour fastness, ease of application, and simple dyeing process coupled with their good reproducibility, reactive dyes find great use with over 50% of the world's consumption [1]. The molecular structure of reactive dyes consists of a chromophoric group and a functional group that can form covalent bonds with cellulosic fibres [2]. Remazol Brilliant Violet 5R (RBV5R) is an example of a reactive dye, which has characteristics of bright colour, simple application techniques, low-energy consumption in the dying process, and high solubility in water [3]. RBV5R

* Corresponding author.

is used widely in fabric manufacturing and as an initiator in the production of polymer dyes. RBV5R is an anthracene derivative and thus a member of an important class of toxic and recalcitrant organic contaminants [4]. When RBV5R enters the aquatic environment, it can be toxic to aquatic life because it prevents photosynthesis by blocking the entry of sunlight into deeper layers [5]. Moreover, this group of dyes is also carcinogenic, mutagenic, toxic, and teratogenic for humans, fish species, and even microorganisms [6]. This type of dye is difficult to eliminate either by biodegradation or sludge adsorption because of its stable conjugated structure [7]. Thus, an effective method of eliminating and decreasing its effect on industrial discharges before mixing with water bodies is vital.

Recently, various methods that include photodegradation [8], ion-exchange oxidation [9], membrane separation [10], and adsorption [11] were reported to efficiently remove dyes from wastewater. Adsorption has been reported to be the most widely used method due to its effectiveness and sustainability. Various adsorbents such as active carbon nanoparticles [12], chitosan [13], carboxymethyl cellulose [14], and perovskite-type oxides [15] have been reported by many studies. Among the large number of adsorbents, activated carbon exhibited advantages over other adsorbents because of its higher adsorption capacity when used on wastewater with different dye molecules. It is well known that activated carbon materials have a porous structure and high surface area. Porosity, size of the specific surface area, and chemical properties of activated carbon are the main factors that determine the adsorption process of organic dyes [16]. Activated carbon has been used in many applications such as gas purification [17], domestic and industrial wastewater treatment [18], water purification [19], medicine [20], sewage treatment, and as filters in compressed air [21]. The preparation of activated carbons has been investigated by many researchers, and they are produced on a commercial scale [22]. However, the production of activated carbon is well known for its high cost. Therefore, many attempts have been made to investigate the utilization of low-cost raw materials to produce activated carbon in order to reduce the total cost involved in activated carbon processing.

Heaps of sawdust get created on a regular basis at sawmills, which consequently continue to create a solid waste management problem at sawmills. About 20,000 m^3 of the wood wastes were still disposed of directly or by burning [23]. Sawdust can be regarded as one of the sustainable sources of organic precursors, because it is generated in a very short period of time and can produce activated carbon from diverse types of wood. The main content of lignocellulosic chemicals and well-structured fibrous constituents of wood has a substantial impact on the preparation of activated carbons [24]. Previous studies have used sawdust from different sources of wood (e.g., *Tectona grandis* [25], fir wood sawdust [26], pine sawdust [27], beech [28], and sapelli wood [29]) as precursors for activated carbon production. Melunak and rubberwood are both categorized as light hardwoods with densities of 530–755 and 560–640 kg/m^3, respectively. The two wood species are among commercially important hardwoods used in the wooden furniture manufacturing industry, with a high consumption of logs recorded. To the best of our knowledge, there has not been any work found in the scientific literature on RBV5R dye removal using activated carbon derived from melunak and rubberwood, which were produced via microwave heating. Herein, we present microwave induced KOH activation of melunak and rubberwood sawdust for the adsorption of RBV5R dye from aqueous solution. Both adsorbents have been characterized by surface chemistry, morphology, surface area and pore structure, and proximate and ultimate analysis. The effect of operating parameters such as the initial pH, contact time, and initial dye concentration has been studied in a batch adsorption experiment. The adsorption isotherm, kinetics, thermodynamic and desorption studies were investigated comprehensively.

2. Materials and methods

2.1. Adsorbent and adsorbate

Melunak (*Pentace* spp.) and rubberwood (*Hevea brasiliensis*) sawdust was collected from a local timber manufacturing plant located in Sungai Petani, Kedah, Malaysia. The sawdust was rinsed with tap water to remove dirt particles, dried at 110°C for 24 h to remove moisture, and then sieved to sizes of 0.5–1 mm. The RBV5R dye was supplied by Merck (M) Sdn. Bhd, Malaysia.

2.2. Preparation of MAC and RAC

For the preparation of MAC and RAC, a two-step technique was applied using carbonization followed by microwave activation with potassium hydroxide (KOH) as the chemical agent. First, the dried MAC and RAC were carbonized to transform them into char material through heating at 700°C for 2 h inside a furnace under 150 cm^3/min of nitrogen (N_2) flow. Second, the melunak and rubberwood char produced was soaked with KOH before heating in a modified microwave oven equipped with carbon dioxide (CO_2) gasification. Melunak char was activated with a KOH:char ratio of 0.86 g/g at 376 W in 4.3 min; while rubberwood char was activated with a KOH:char ratio of 0.75 g/g at 430 W in 4.8 min. The KOH:char ratio, power, and time used were chosen based on the optimum conditions where the maximum RBV5R removal and yield were achieved. The obtained MAC and RAC were washed using deionized water until a neutral pH was attained before drying at 110°C in an oven.

2.3. MAC and RAC characterization

The proximate analyses were conducted using a simultaneous thermal analyser STA 6000 M/s PerkinElmer, USA. The elemental composition of C, H, N, S, and O of precursors and activated carbons was analysed using an elemental analyser, 2400 Series II M/s PerkinElmer, USA. The nitrogen adsorption–desorption isotherm was conducted at 77 K using a Micromeritics ASAP 2010 sorptometer applying the Brunauer–Emmett–Teller (BET) method for specific surface area and the Barrett–Joyner–Halenda (BJH) method for pore size distribution. The *t*-plot method was

used to determine the micropore volume. The morphologies of MAC and RAC were characterized using scanning electron microscopy (SEM) on a SUPRA 55VP M/s Carl Zeiss AG, Germany. The occurrence of functional groups was assessed using Fourier transform infrared spectroscopy, with an IR Prestige 21 M/s FTIR spectrometer, Shimadzu, Japan.

2.4. Batch experiments

The batch adsorption experiments were conducted in a set of 250 mL of Erlenmeyer flasks containing 200 mL of RBV5R dye solution, and 0.2 g of MAC and RAC were added to each flask. The flasks were agitated at 120 rpm using a shaker until the equilibrium was reached. The effect of temperature on the adsorption process was investigated at different temperatures ranging from 30°C to 60°C at a constant initial concentration of 100 mg/L of RBV5R dye solutions and pH 7. The pH was adjusted by adding a suitable amount of 0.1 M HCl or NaOH. The effects of the initial adsorbate concentration and contact time on the adsorption process were assessed using RBV5R dye solution concentrations ranging from 25 to 300 mg/L at a constant pH of 7 and a temperature of 30°C until the equilibrium stage was attained. The effect of pH was evaluated at pH 2, 4, 6, 8, 10, and 12 in a solution of 100 mg/L of dye, keeping the temperature at 30°C.

3. Results and discussion

3.1. Characterization of MAC and RAC

Fig. 1a and b show the proximate analysis of the precursors and the activated carbons, respectively. Both precursors show a high content of volatile matter (VM) followed by fixed carbon (FC), moisture content, and ash. The low ash and high VM demonstrated that both precursors are suitable for activated carbon production [30]. After employing activation, it can be seen that the FC content was dominant for MAC and RAC, about 78.31% and 70.39%, respectively. The elemental analysis results are shown in Figs. 1c and d. The percentages of elemental carbon in the precursors were only 33.44% and 22.46% before they increased to 79.34% and 70.73% for MAC and RAC, respectively.

The porous characteristics of the precursors as well as the activated carbon produced are summarized in Table 1. The porous characteristics of MAC and RAC were improved as compared with the precursor material, implying the development of additional pores during the microwave irradiation stage. The BET surface area of MAC is higher than the surface area of RAC. It was evident that the mesopores of MAC and RAC account for about 75.1% and 62.1% of the total pore volume, with a well-developed porous structure.

The pore size distribution and the adsorption/desorption isotherms of MAC and RAC are shown in Figs. 2a

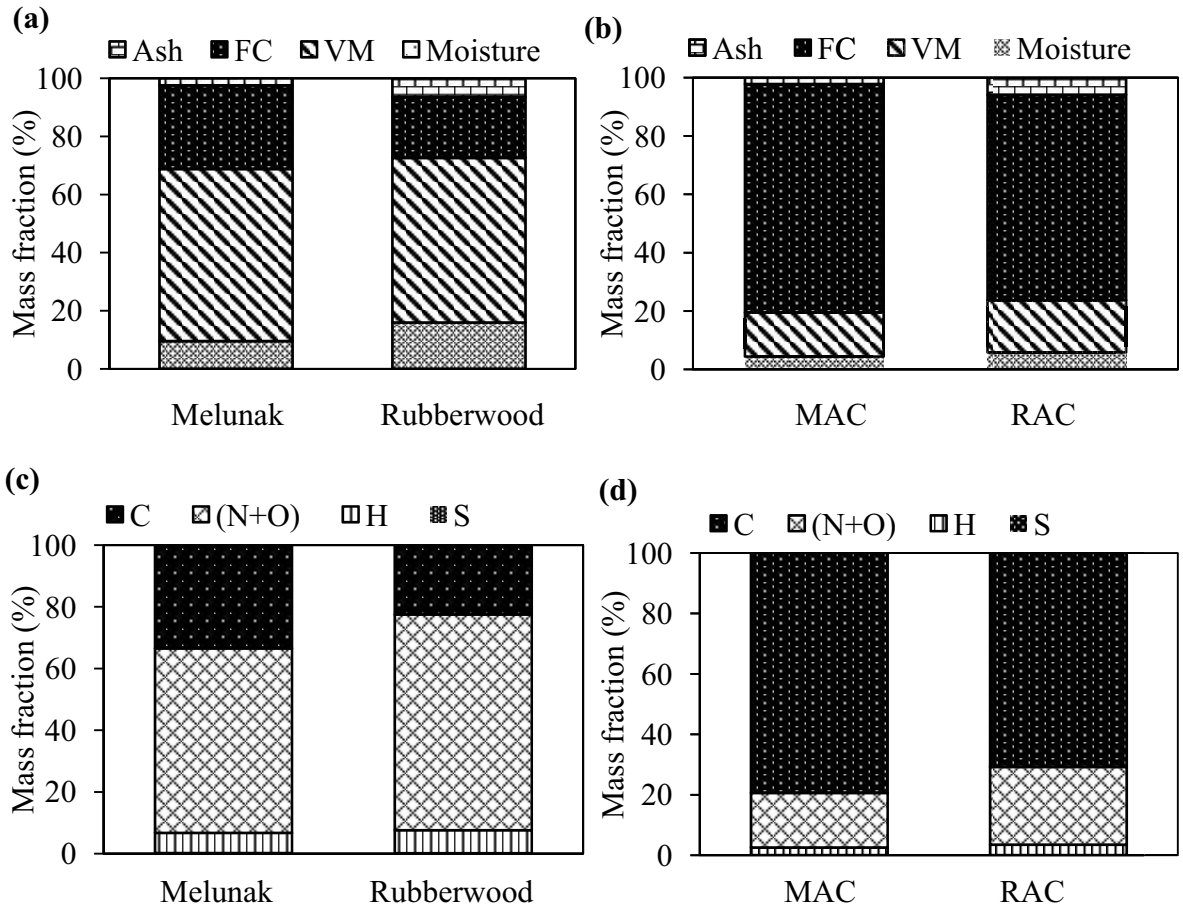

Fig. 1. Proximate analysis of (a) precursor and (b) activated carbons, and elemental analysis of (c) precursor and (d) activated carbons.

Table 1
Porosity structures of the precursors and activated carbons

Properties	Melunak	Rubberwood	MAC	RAC
BET surface area (m^2/g)	13.4	5.1	914.0	796.0
Total pore volume (cm^3/g)	0.0137	0.0087	0.522	0.422
Micropore volume (cm^3/g)	0.0027	0.0003	0.130	0.160
Mesopore volume (cm^3/g)	0.0110	0.0084	0.392	0.262
Average pore diameter (nm)	2.98	2.50	3.20	3.10

and b, respectively. From the figures, the pore diameter distribution for both MAC and RAC lies between 1.63 and 43 nm. This indicates that both activated carbons consist of a mesoporous structure with few micropores. The average pore diameter for MAC and RAC are 3.20 and 3.10, respectively. The adsorption–desorption profiles of MAC and RAC in Fig. 2 show hysteresis loops, and they were fitted to type IV isotherms, which implied the existence of well-developed micropores and mesopores according to IUPAC classification. The hysteresis loop can be classified as an H4 loop, which is related to narrow slit-like pores [31].

The morphology of melunak and rubberwood before and after activation in producing MAC and RAC was characterized using SEM. From the morphology, the surface textures of the raw melunak and rubberwood were irregular and rough. After activation, different sizes and shapes of pores can be observed on the surface of MAC and RAC. This indicates that there are possibilities for the RBV5R molecule to be adsorbed and trapped into many of the pores present on both the MAC and RAC surfaces. The pores formed after the carbonization process were originally from the empty spaces formerly occupied by the moisture and the VM components.

These components are unable to endure heat; so they evaporate and leave the samples. Some new pores are produced due to the activation process using microwave irradiation plus KOH and also from CO_2 gasification [32].

The sawdust can be seen to exhibit a variety of functional groups on its surface. The IR spectrum of melunak revealed the presence of O–H (3,611–3,951 cm^{-1}), C–H (2,720 cm^{-1}), C≡C (2,335 cm^{-1}), C=O (1,689 cm^{-1}), C=C (1,520 cm^{-1}), and C–O (1,269 cm^{-1}) stretching vibrations [33]. Some peaks in the MAC spectrum were seen to disappear or shift, leaving only O–H groups at 3,800 cm^{-1} and a carboxyl group peak at 1,615 cm^{-1} due to volatilization during KOH chemical activation [34]. The FTIR spectrum of rubberwood sawdust revealed peaks at 3,524–3,947 cm^{-1}, which are attributed to the occurrence of O–H stretching bands from hydroxyl groups. The peak at 2,320 cm^{-1} relates to the occurrence of a C–H group (alkanes). Other peaks detected at bandwidths of 1,520 and 1,702 cm^{-1} are both attributed to the existence of a carboxyl (C=O) group. Similar to MAC, many peaks have been lost in the RAC IR spectrum, leaving the peak at 3,791 cm^{-1}, which relates to the existence of hydroxyl (O–H) groups, and a band at 1,716 cm^{-1}, which corresponds to stretching of the carboxyl (C=O) group. The intensity of most of the peak was reduced or even disappeared after activation, signifying the dehydrating activities of KOH during activation process [35].

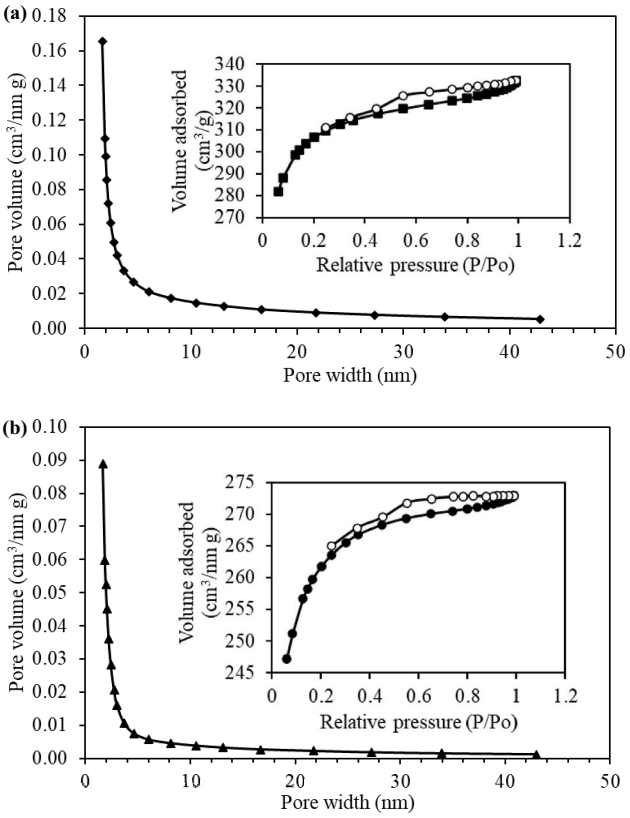

Fig. 2. Pore size distribution and N_2 adsorption (filled symbols) and desorption (open symbols) isotherms (inset plot) of (a) MAC and (b) RAC.

3.2. Influence of initial pH

The initial pH is one of the most important factors that can affect the adsorption capacity, the charges present on the surface of the adsorbent, and the solubility of the dyes [36]. The influence of pH on RBV5R adsorption onto both MAC and RAC was studied at 30°C with 100 mg/L RBV5R solution over the pH range of 2–12. The results are depicted in Fig. 3a where both curves can be seen to follow the same trends. With increasing the RBV5R solution pH from 6 to 12, the adsorption capacity of MAC and RAC toward RBV5R dye was gradually reduced. At higher pH values, the electrostatic repulsion among the negatively charged surface sites on the adsorbent and the anionic dye increased in basic conditions. Besides, the excess OH^- ions

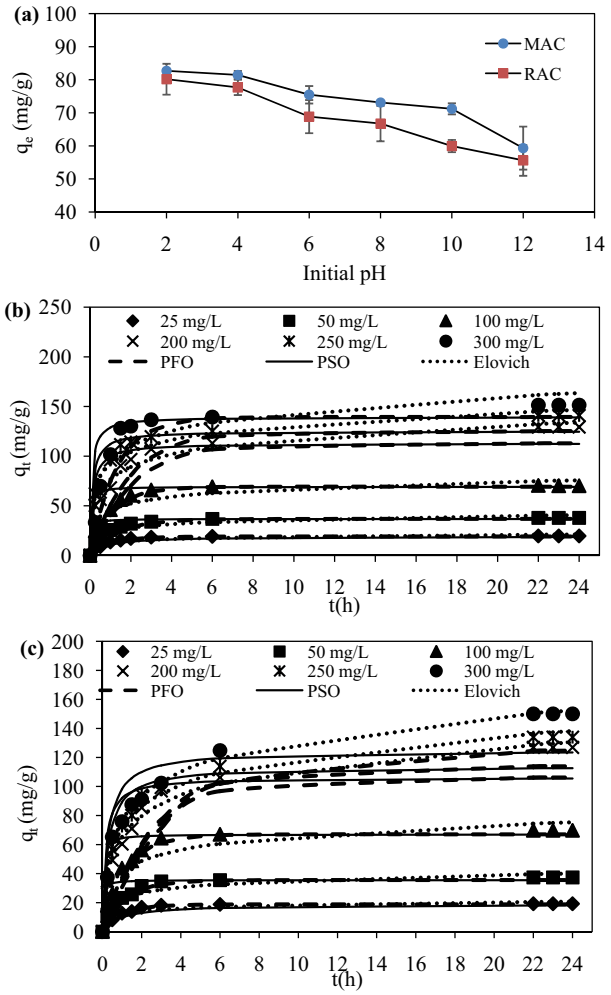

Fig. 3. Influence of (a) initial pH, (b) contact time and kinetics for RBV5R adsorption on MAC and (c) contact time and kinetics for RBV5R adsorption on RAC.

competed with RBV5R ions for the available positively charged adsorption sites [37]. The maximum adsorption capacity of RBV5R was obtained at pH 2 (acidic condition), where the hydroxyl (–OH) and carboxyl (–COOH) groups on the surface of MAC and RAC were protonated and became more positively charged. The adsorption capability was, therefore, higher under this condition due to the strong electrostatic interaction between the negatively charged RBV5R molecules and the positively charged MAC and RAC in acidic conditions.

3.3. Influence of initial concentration, contact time, and adsorption kinetics on adsorption

Figs. 3b and c illustrate the influence of the initial concentration and contact time on RBV5R adsorption by MAC and RAC, respectively. The adsorption process takes place in two successive stages: (i) a rapid initial stage, which implies strong electrostatic attractions between RBV5R and the adsorbent surface, and (ii) a stable stage (equilibrium) with no significant improvement in the adsorption, meaning saturation of the active sites in MAC and RAC. As the RBV initial concentration increased from 25 to 300 mg/L, RBV uptake was found to rise from 19.61 to 151.50 mg/g and 19.20 to 150.02 mg/g for RBV-MAC and RBV-RAC, respectively. A shorter time of 1 to 2 h was required by lower RBV initial concentrations of 25, 50, and 100 mg/L to complete the adsorption process and to attain the equilibrium state. Whereas for higher RBV initial concentrations of 200, 250, and 300 mg/L, longer times of 8–10 h and 22–23 h were needed for MAC and RAC, respectively. To make sure of sufficient contact time, further batch experiments were carried out for 24 h.

This indicates that MAC facilitates the uptake ability better than RAC at a higher initial concentration. This can be explained by the high surface area and porous structure and the fact that there is high driving force induced by the concentration gradient for dye transfer from the aqueous solution to the interior micro- and mesopores of the adsorbent at high initial concentrations [38].

The experimental data were fitted to different kinetic models using the pseudo-first-order (PFO) [39], pseudo-second-order (PSO) [40], and Elovich [41] models. The parameters of PFO, PSO, and Elovich models are listed in Table 2. With respect to the magnitude of R^2 values, PSO kinetic models well described the adsorption of RBV5R onto both adsorbents MAC and RAC (Figs. 3b and c). Moreover, the $q_{e,\exp}$ values agreed satisfactorily with the $q_{e,\text{cal}}$ values, which resulted in Δq ranging from 5.66% to 14.88% and 3.25% to 17.85% for RBV adsorption by MAC and RAC, respectively. Some of the adsorption systems were found to be better represented by the Elovich equation, giving Δq values, which were lower than those obtained from the PSO model. However, if considering only their R^2 values, the PSO model was still the best equation to describe the kinetics of all the adsorption systems. This implies that the adsorption of RBV5R onto both MAC and RAC occurred predominantly by chemisorption. The PSO model assumes that the chemical reaction between adsorbent and adsorbate controls the rate of adsorption process [35].

3.4. Adsorption isotherm

Adsorption isotherms are useful tools for understanding the behaviour of adsorption processes when the system is in equilibrium. In this study, the two-parameter isotherm models of Langmuir, Freundlich, and Temkin [42] and the three-parameter isotherm models of Dubinin–Radushkevich, Redlich–Peterson, and Toth [36] were fitted to the experimental data of RBV5R adsorption onto MAC and RAC.

The different isotherm parameters along with the R^2 and χ^2 values are given, respectively, in Table 3. For both MAC and RAC, it can be seen that Langmuir, Redlich–Peterson, and Toth isotherm models give high R^2 values (>0.99). Therefore, to determine the best model among these three models, considering the χ^2 values is also vital. With the lowest value of chi-square ($\chi^2 = 1.29$), the Langmuir isotherm model had a better fit to the RBV adsorption onto the MAC experimental data compared with the other isotherm models. The excellent fit of

Table 2
Kinetic parameters for RBV5R adsorption on MAC and RAC

Adsorbent	C_0 (mg/L)	$q_{e,exp}$ (mg/g)	PFO model			PSO model			Elovich model			
			k_1 (1/h)	q_e (mg/g)	R^2	k_2 (g/mg h)	q_e (mg/g)	R^2	α (mg g^{-1} h^{-1})	β (g mg^{-1})	q_e (mg/g)	R^2
MAC	25	19.61	0.90	15.77	0.9970	0.07	22.52	0.9953	398.44	0.39	21.10	0.8201
	50	37.86	0.70	27.10	0.9729	0.57	40.00	0.9999	615.55	0.20	40.54	0.8555
	100	70.15	0.88	57.13	0.9960	0.35	75.19	0.9999	1213.91	0.11	75.72	0.8231
	200	129.37	0.49	90.49	0.9771	0.07	136.99	0.9988	1284.11	0.06	133.80	0.9502
	250	140.99	0.52	82.80	0.8924	0.07	156.25	0.9985	3,754.54	0.06	146.62	0.9049
	300	151.50	0.77	112.02	0.9018	0.09	169.49	0.9990	1,750.86	0.05	163.59	0.7960
RAC	25	19.20	0.93	17.10	0.9866	0.06	22.62	0.9859	278.46	0.38	20.68	0.8301
	50	37.39	0.82	33.14	0.9869	0.84	38.61	0.9999	372.49	0.18	40.06	0.8631
	100	69.78	0.81	64.53	0.9928	0.36	74.07	0.9999	499.26	0.09	75.31	0.8599
	200	126.96	0.40	98.80	0.9910	0.06	135.14	0.9977	497.24	0.05	130.43	0.9811
	250	133.95	0.38	96.17	0.9324	0.03	156.25	0.9935	632.43	0.05	138.22	0.9795
	300	150.02	0.28	104.03	0.9095	0.03	175.44	0.9950	582.42	0.04	152.44	0.9923

Table 3
Two- and three-parameter isotherm models for adsorption of RBV5R onto MAC and RAC

Isotherm type	Model	Parameter	Adsorbent	
			MAC	RAC
Two-parameter isotherm	Langmuir	Q_m (mg/g)	238.33	204.08
		K_L (L/mg)	0.019	0.018
		R^2	0.9913	0.9908
		χ^2	1.29	1.22
	Freundlich	K_F (mg/g (L/mg)$^{1/n}$)	7.53	7.17
		n_F	1.59	1.58
		R^2	0.9797	0.9763
		χ^2	7.74	7.95
	Temkin	A_T	0.24	0.22
		B_T (L/g)	42.80	42.03
		R^2	0.9749	0.9786
		χ^2	12.71	9.17
Three-parameter isotherm	Dubinin–Radushkevich	E (kJ/mol)	0.22	0.22
		Q_{DR} (mg/g)	126.78	105.61
		R^2	0.7689	0.7860
		χ^2	247.46	57.79
	Redlich–Peterson	K_R (L/g)	3.10	3.15
		α_R (1/mg)g	0.0023	0.0041
		g	1.36	1.26
		R^2	0.9958	0.9934
		γ^2	3.48	0.99
	Toth	Q_T	329.37	281.07
		b_T	0.010	0.012
		n_T	2.65	0.99
		R^2	0.9960	0.9932
		γ^2	3.11	0.89

the Langmuir isotherm to the experimental adsorption data confirms that the adsorption is monolayer; the adsorption of each molecule has equal activation energy and sorbate–sorbate interaction is negligible. As for RAC, the Toth model was found to better describe the adsorption process than the others, considering the higher correlation coefficient values (R^2 = 0.9932) and low chi-square (χ^2 = 0.89) that it showed. The Toth isotherm, derived from potential theory, has proven useful in describing sorption in heterogeneous systems such as phenolic compounds on carbon [36]. When n_T = 1 in the Toth equation, this isotherm is reduced to the Langmuir adsorption isotherm equation. The n_T value for RAC approximates unity, thus reverting it to the original Langmuir equation. The highest adsorption capacities were determined using the Toth model with Q_T of 329.37 and 281.07 mg/g for MAC and RAC, respectively. However, the Langmuir adsorption capacity, Q_m, is closest to the experimental value for MAC and RAC, which are 151.50 and 150.02, respectively.

The adsorption capacities of RBV5R onto MAC and RAC estimated by the Langmuir model were 238.33 and 204.08 mg/g, respectively. These values seem high compared with other adsorbents in the literature, which used green coconut mesocarp [43] and cocoa pod husks [44] with maximum adsorption capacities of 7.28 and 76.92 mg/g, respectively. The relatively high adsorption capacity suggests good adsorption efficiency of the MAC and RAC for RBV5R adsorption.

3.5. Adsorption mechanism

The kinetic data were further investigated by using Weber–Morris intraparticle diffusion [45] and Boyd [35] models to establish the actual rate-controlling step. The intraparticle plots for RBV adsorption by MAC and RAC at 30°C are shown in Figs. 4a and c, respectively. Multilinear lines with three different regions are spotted on this plot, indicating that intraparticle diffusion was not the only rate limiting step involved in the sorption process. The first stage, starting from the origin, is related to the transfer of adsorbate molecules from bulk liquid to the external surface of adsorbent. The second stage indicates intraparticle diffusion. The third linear part indicates the equilibrium

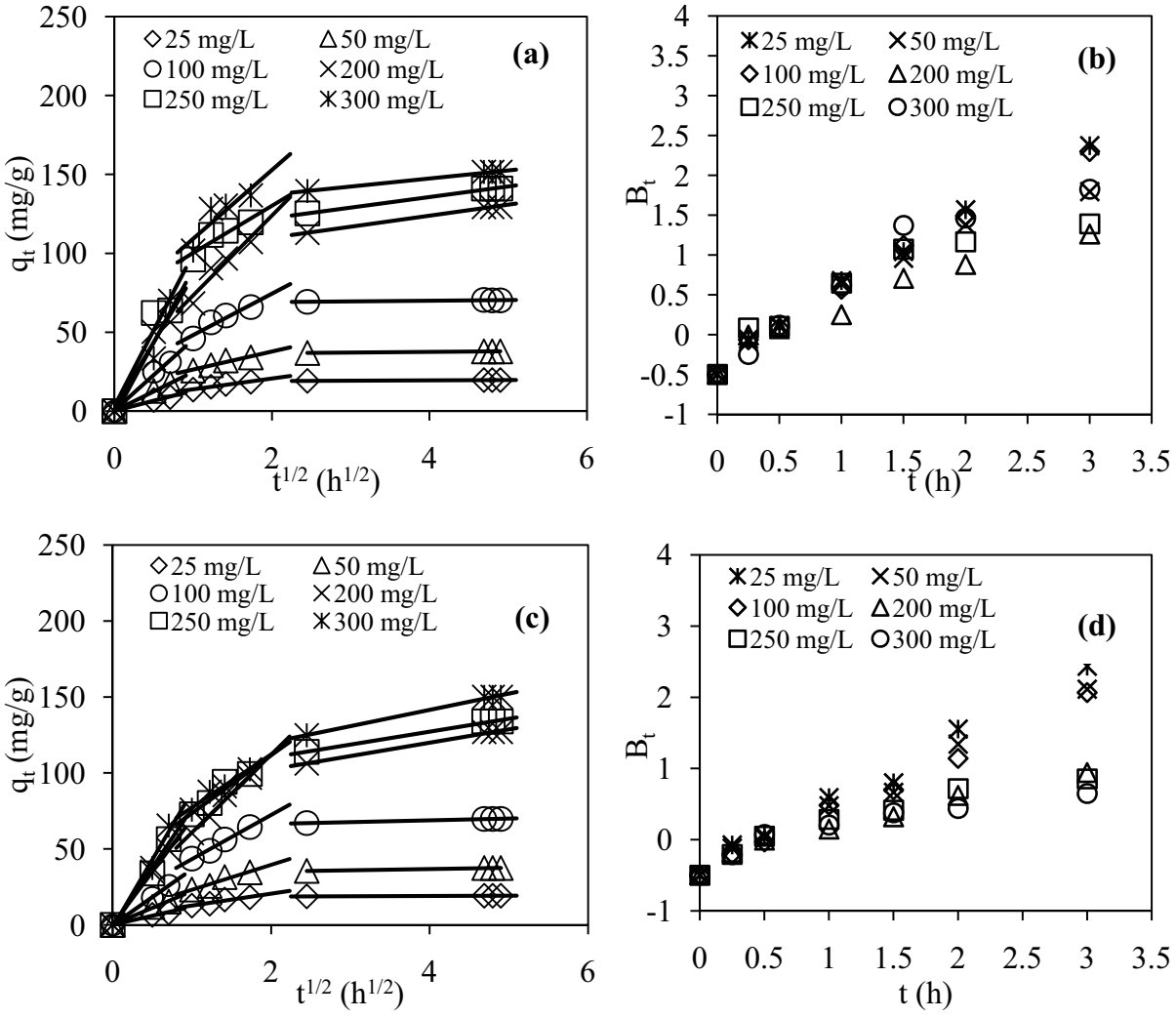

Fig. 4. Intraparticle diffusion plot and Boyd plot of MAC (a and b) and RAC (c and d).

phase [46]. The k_{ti} values for all three regions increased as the RBV initial concentrations increased. Higher k_{ti} values were obtained due to the greater driving force for mass transfer that developed at higher initial concentrations. Besides k_{ti}, the values of C_i were found to increase too at higher initial concentrations for all three regions, therefore confirming an increase in boundary layer thickness.

The Boyd kinetic model was employed to identify whether the rate limiting step of adsorption is film diffusion or intraparticle diffusion. As shown in Figs. 4b and d, although the Boyd's plots present some linearity, they do not pass through the origin. Therefore, film diffusion or a chemical reaction controlled the adsorption rate of RBV onto MAC and RAC. The slopes (B), which were obtained from the linear portions of the plots, and the effective diffusion coefficients (D_i), calculated from the B values, are presented in Table 4.

Diffusion coefficients in the order of 10^{-6} to 10^{-8} are found when the rate is governed by film diffusion; whereas the diffusion coefficients are in the order of 10^{-11} to 10^{-13} when the rate is controlled by pore diffusion [47]. The D_i for both MAC and RAC is in the order of 10^{-8}, thus proving that film diffusion is the rate-limiting step controlling adsorption.

3.6. Pore filling and possible interaction

Pore filling was predominantly responsible for the adsorption mechanism together with several possible interactions. The molecule length of RBV5R dyes is shown in Fig. 5. From the figure, RBV5R dye molecules have a crowded charge centre and a large molecular size (2.12 × 1.09 nm). From pore analysis, MAC and RAC contain 75.1% and 62.1% mesopore volume, respectively. The remaining consists of micropore structure. The pore diameter distribution of MAC and RAC lies between 1.63 and 43 nm. Therefore, RBV can enter most mesopores, which have a size greater than 2.12 nm, but it cannot fill into most micropores. Hence, MAC has higher adsorption capacity and removal efficiency when compared with RAC.

From the surface chemistry results, MAC and RAC show the presence of an O–H group (alcohols and phenols) and a carboxyl (C=O) group. There are three possible interaction mechanisms for the adsorption of RBV5R onto MAC and RAC, namely, hydrogen bonding, n–π interactions, and π–π interactions as shown in Fig. 5b. Hydrogen bonding interactions occurred between hydroxyl groups of MAC and RAC with the H acceptor oxygen atom. The n–π interactions occurred between the oxygen group on the ACs surface with the aromatic ring of the RBV5R dye molecule. The π–π interactions occurred between the π-electrons in a carbonaceous adsorbent and the π-electron in the aromatic ring of an adsorbate.

3.7. Adsorption thermodynamic studies

The most common equations that relate thermodynamic parameters such as changes in free energy (ΔG°), enthalpy (ΔH°), and entropy (ΔS°) can be estimated by the change of equilibrium constants with temperature. The values of ΔH° and ΔS° were calculated using the following equation of Van't Hoff:

$$\ln K_L = \frac{\Delta S^\circ}{R} - \frac{\Delta H^\circ}{RT} \tag{1}$$

ΔG° can be calculated below by using the relation:

$$\Delta G^\circ = -RT\ln K_L \tag{2}$$

The values of E_a were calculated using the following equation:

$$\ln k_2 = \ln A - \frac{E_a}{RT} \tag{3}$$

where R is the constant of a perfect gas (R = 8.314 J/mol K); T is the absolute temperature of solution (K); K_L is the Langmuir isotherm constant (L/mg); k_2 is the pseudo-second-order

Table 4
Diffusion mechanism for RBV5R adsorption on MAC and RAC

		Intraparticle diffusion model									Boyd plot	
Adsorbent	C_0 (mg/L)	k_{t1}	C_1	R^2	k_{t2}	C_2	R^2	k_{t3}	C_3	R^2	B	D_i (m²/h)
MAC	25	12.84	0.14	0.9923	6.79	7.03	0.9708	0.18	18.74	0.9948	0.93	9.46E-08
	50	24.71	0.09	0.9992	11.46	14.83	0.9534	0.43	35.78	0.9948	0.76	7.69E-08
	100	44.81	0.53	0.9904	26.21	21.99	0.9345	0.43	68.16	0.9056	0.92	9.27E-08
	200	83.60	1.92	0.9644	50.55	41.31	0.9053	6.96	95.98	0.9948	0.55	5.55E-08
	250	96.55	3.15	0.9305	29.95	70.24	0.8428	6.68	108.92	0.9948	0.61	6.16E-08
	300	92.82	2.95	0.9342	43.58	65.65	0.7637	5.11	126.98	0.9948	0.82	8.29E-08
RAC	25	11.85	0.16	0.9869	7.84	4.88	0.9492	0.17	18.41	0.9948	0.95	9.60E-08
	50	22.04	0.18	0.9954	16.37	6.80	0.9526	0.79	33.62	0.9948	0.84	8.53E-08
	100	36.68	0.06	0.9998	29.08	14.22	0.9911	1.18	64.12	0.9948	0.82	8.34E-08
	200	69.75	0.03	1.0000	51.24	9.63	0.9800	8.81	84.70	0.9948	0.45	4.53E-08
	250	77.59	1.12	0.9855	38.11	35.44	0.9271	8.49	93.20	0.9948	0.43	4.40E-08
	300	89.13	1.60	0.9779	34.93	42.35	0.9765	10.69	98.71	0.9948	0.35	3.50E-08

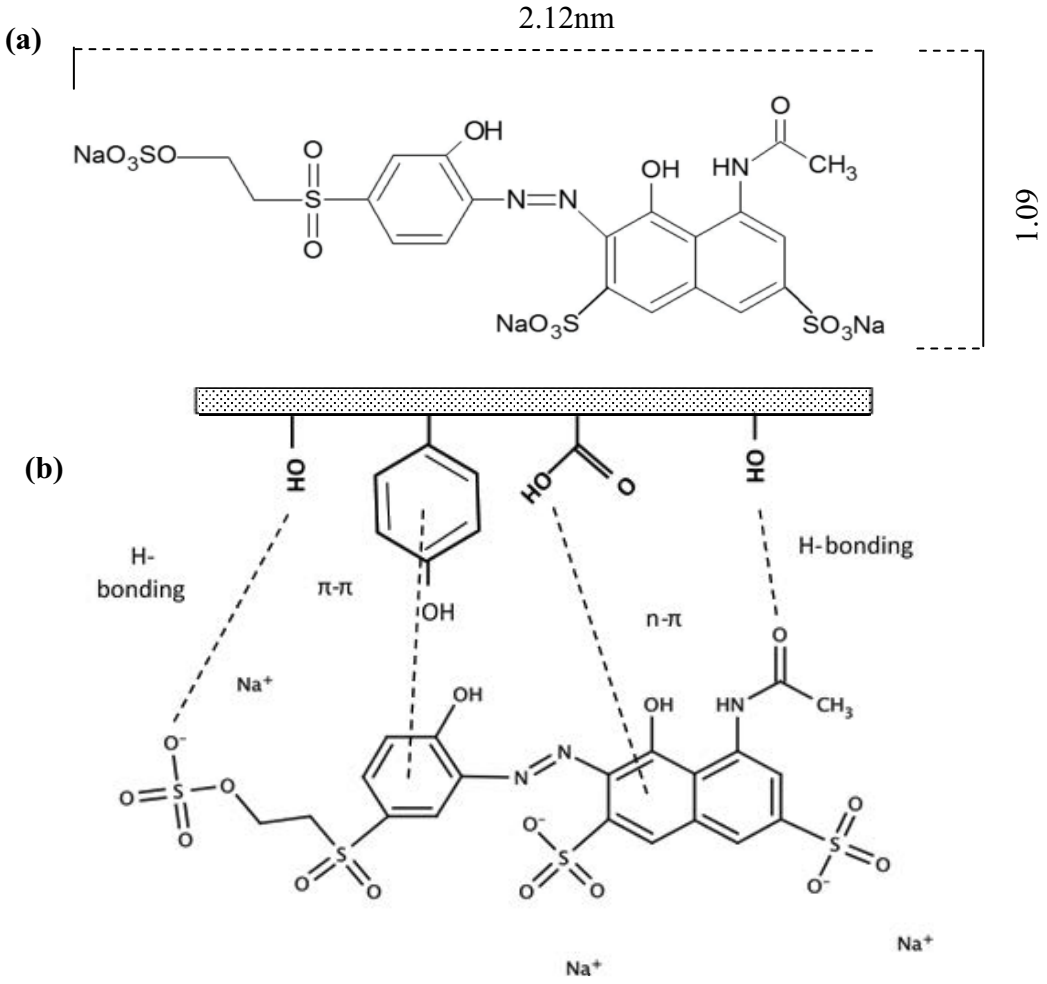

Fig. 5. (a) Molecular dimension of RBV5R and (b) possible interaction mechanisms for RBV5R dye adsorption onto MAC and RAC.

rate constant (g/mg h); E_a is the activation energy (kJ/mol); and A is the Arrhenius pre-exponential factor.

The calculated parameters of $\Delta H°$, $\Delta S°$, $\Delta G°$, and E_a are shown in Table 5. The positive values of $\Delta H°$ confirmed the endothermic nature of the RBV5R adsorption onto both MAC and RAC. Meanwhile, the positive value of the entropy change ($\Delta S°$) for both adsorbents can be ascribed to the increasing randomness and the good binding affinity of RBV5R toward the adsorbents. On the other hand, the free energy change, $\Delta G°$, values for the two adsorbents are negative, illustrating that the adsorption processes were feasible and spontaneous in the temperature range studied. Lower values of activation energy, E_a (5–40 kJ/mol) suggest a physisorption mechanism of adsorption, whereas higher values (40–800 kJ/mol) are related to chemisorption processes [48]. The E_a values of 10.48 and 6.78 kJ/mol for MAC and RAC, respectively, confirm the physisorption nature of RBV adsorption.

The Langmuir and pseudo-second-order model for isotherm and kinetic studies, which were well fitted with the adsorption data for both MAC and RAC represent chemisorption. There are linear relationships between Q_m and BET surface area and total pore volume for both activated carbons, which show that pore filling is the primary mechanism for RBV5R adsorption, which, therefore, is physisorption. However, the values obtained in the thermodynamic studies show lower activation energy for both activated carbons, which represent physisorption. Therefore, the adsorption of RBV dye onto MAC and RAC occurred mainly due to physisorption with some exception of chemisorption. Ribeiro et al. [49] stated that both chemisorption and physisorption can occur simultaneously or alternately.

3.8. Desorption and regeneration studies

The reusability of the spent activated carbons was evaluated by using ethanol as the desorbing agent [50]. After four cycles, the regeneration efficiency for RBV5R removal using MAC and RAC decreased as the cycles progressed. The regeneration efficiencies of MAC onto RBV5R dye for four cycles were 73.30%, 72.44%, 69.35%, and 57.06%; while for RAC they were 65.89%, 63.29%, 60.88%, and 54.93%. The small decrease in the capacity can be attributed to the possible loss of the active sites on the adsorbent. The obtained results indicated that MAC has higher capacity compared with RAC, and this result is consistent with the higher BET surface area of MAC compared with RAC. About 67.06% and 56.93% of the amount of RBV5R adsorbed onto MAC

Table 5
Thermodynamic parameters for RBV5R adsorption onto MAC and RAC

Adsorbent	$\Delta H°$ (kJ/mol)	$\Delta S°$ (kJ/mol)	E_a (kJ/mol)	$\Delta G°$ (kJ/mol)		
				303 K	318 K	333 K
MAC	10.76	0.053	10.48	–5.09	–6.22	–6.64
RAC	8.06	0.044	6.78	–4.96	–6.41	–6.23

and RAC, respectively, was recovered even after the fourth cycling; this confirmed that the synthesized MAC and RAC had good reusability performance.

4. Conclusions

The ability of melunak and rubberwood waste sawdust to remove RBV5R dye in water medium was examined by means of evaluating the following parameters: initial concentration, contact time, and initial pH. In addition, adsorption kinetics, isotherm, mechanism, and thermodynamic studies have also been developed. The isotherm adsorption data were described well by the Langmuir isotherm model, which describes monolayer adsorption on a homogeneous surface for MAC and RAC. The surface area of MAC (914 m^2/g) was found to be greater than RAC (796 m^2/g). The Fourier transformed infrared (FTIR) spectra indicated the presence of hydroxyl (O–H) and carboxyl (C=O) groups in both of the adsorbents. The PSO model was the most suitable fit to the adsorption kinetic data owing to the higher R^2 and smaller deviations between the calculated and experimental values (q_e) for both adsorbents. The film diffusion rate was found to limit the rate of adsorption. The thermodynamic study revealed that the adsorption of RBV5R was endothermic and physisorption in nature. The proposed results confirmed the promising ability of MAC and RAC for the removal of hazardous dyes from wastewater.

Acknowledgements

The author would like to acknowledge the support from the Fundamental Research Grant Scheme (FRGS) under a grant number of FRGS/1/2019/STG07/UNIMAP/02/2 from the Ministry of Higher Education Malaysia.

References

[1] M.N. Amin, R.S. Blackburn, Sustainable chemistry method to improve the wash-off process of reactive dyes on cotton, ACS Sustainable Chem. Eng., 3 (2015) 725–732.
[2] I.A. Umar, G. Abdulraheem, S. Bala, S. Muhammad, Kinetics, equilibrium and thermodynamics studies of C.I. Reactive Blue 19 dye adsorption on coconut shell based activated carbon, Int. Biodeterior. Biodegrad., 102 (2015) 265–273.
[3] M.F. Hanafi, N. Sapawe, Effect of initial concentration on the photocatalytic degradation of remazol brilliant blue dye using nickel catalyst, Mater. Today Proc., 31 (2020) 318–320.
[4] O.S. Bello, M.A. Ahmad, Removal of Remazol Brilliant Violet-5R dye using periwinkle shells, Chem. Ecol., 27 (2011) 481–492.
[5] E. Rápó, L.E. Aradi, Á. Szabó, K. Posta, R. Szép, S. Tonk, Adsorption of Remazol Brilliant Violet-5R textile dye from aqueous solutions by using eggshell waste biosorbent, Sci. Rep., 10 (2020) 8385.
[6] P.V. Thitame, S.R. Shukla, Adsorptive removal of reactive dyes from aqueous solution using activated carbon synthesized from waste biomass materials, Int. J. Environ. Sci. Technol., 13 (2016) 561–570.
[7] X. Li, X. Xie, H. Luo, L. Li, Z. Li, Z. Xue, W. Li, Adsorption of reactive yellow X-RG and reactive brilliant red X-3B onto cucurbit[8]uril and cucurbit[6]uril: effect factors, adsorption behavior and mechanism study, J. Colloid Interface Sci., 498 (2017) 31–46.
[8] S. Zhou, Z. Fu, L. Xia, Y. Mao, W. Zhao, A. Wang, C. Zhang, C. Ding, W. Xu, In situ synthesis of ternary hybrid nanocomposites on natural Juncus effusus fiber for adsorption and photodegradation of organic dyes, Sep. Purif. Technol., 255 (2021) 117671.
[9] J. Joseph, R.C. Radhakrishnan, J.K. Johnson, S.P. Joy, J. Thomas, Ion-exchange mediated removal of cationic dye-stuffs from water using ammonium phosphomolybdate, Mater. Chem. Phys., 242 (2020) 122488.
[10] C. Ao, J. Zhao, T. Xia, B. Huang, Q. Wang, J. Gai, Z. Chen, W. Zhang, C. Lu, Multifunctional $La(OH)_3$@cellulose nanofibrous membranes for efficient oil/water separation and selective removal of dyes, Sep. Purif. Technol., 254 (2021) 117603.
[11] P.M. Thabede, N.D. Shooto, E.B. Naidoo, Removal of methylene blue dye and lead ions from aqueous solution using activated carbon from black cumin seeds, South Afr. J. Chem. Eng., 33 (2020) 39–50.
[12] X. Tao, H. Xu, S. Luo, Y. Wu, C. Tian, X. Lu, Y. Qing, Construction of N-doped carbon nanotube encapsulated active nanoparticles in hierarchically porous carbonized wood frameworks to boost the oxygen evolution reaction, Appl. Catal. B, 279 (2020) 119367.
[13] A. Shalbafan, H. Hassannejad, M. Rahmaninia, Formaldehyde adsorption capacity of chitosan derivatives as bio-adsorbents for wood-based panels, Int. J. Adhes. Adhes., 102 (2020) 102669.
[14] W. Wang, J. Ni, L. Chen, Z. Ai, Y. Zhao, S. Song, Synthesis of carboxymethyl cellulose-chitosan-montmorillonite nanosheets composite hydrogel for dye effluent remediation, Int. J. Biol. Macromol., 165 (2020) 1–10.
[15] L.E. Verduzco, R. Garcia-Díaz, A.I. Martinez, R.A. Salgado, F. Méndez-Arriaga, S.A. Lozano-Morales, M. Avendaño-Alejo, K.P. Padmasree, Degradation efficiency of methyl orange dye by $La_{0.5}Sr_{0.5}CoO_3$ perovskite oxide under dark and UV irradiated conditions, Dyes Pigm., 183 (2020) 108743.
[16] W. Xiao, Z.N. Garba, S. Sun, I. Lawan, L. Wang, M. Lin, Z. Yuan, Preparation and evaluation of an effective activated carbon from white sugar for the adsorption of rhodamine B dye, J. Cleaner Prod., 253 (2020) 119989.
[17] K.M.S. Khalil, O.A.S. Allam, M. Khairy, K.M.H. Mohammed, R.M. Elkhatib, M.A. Hamed, High surface area nanostructured activated carbons derived from sustainable sorghum stalk, J. Mol. Liq., 247 (2017) 386–396.
[18] N.A. Rashidi, S. Yusup, A review on recent technological advancement in the activated carbon production from oil palm wastes, Chem. Eng. J., 314 (2017) 277–290.
[19] S. Sangon, A.J. Hunt, T.M. Attard, P. Mengchang, Y. Ngernyen, N. Supanchaiyamat, Valorisation of waste rice straw for the production of highly effective carbon based adsorbents for dyes removal, J. Cleaner Prod., 172 (2018) 1128–1139.
[20] T. Maneerung, J. Liew, Y. Dai, S. Kawi, C. Chong, C.H. Wang, Activated carbon derived from carbon residue from biomass gasification and its application for dye adsorption: kinetics,

isotherms and thermodynamic studies, Bioresour. Technol., 200 (2016) 350–359.
[21] N. Syuhada, R. Hashim, M. Hazim, M. Amini, M. Danish, O. Sulaiman, Optimization of activated carbon preparation from cassava stem using response surface methodology on surface area and yield, J. Cleaner Prod., 198 (2018) 1422–1430.
[22] S.H. Kow, M.R. Fahmi, C.Z.A. Abidin, S.A. Ong, N. Ibrahim, Regeneration of spent activated carbon from industrial application by NaOH solution and hot water, Desal. Water Treat., 57 (2016) 29137–29142.
[23] T. Yoshida, H. Suzuki, Current Status of Woody Biomass Utilization in ASEAN Countries, InTech, 2010, pp. 113–124.
[24] M. Danish, T. Ahmad, A review on utilization of wood biomass as a sustainable precursor for activated carbon production and application, Renewable Sustainable Energy Rev., 87 (2018) 1–21.
[25] I. Pestana, C. Ramiro, P. Alexandre, M. Mourão, Valorisation of *Tectona grandis* tree sawdust through the production of high activated carbon for environment applications, Bioresour. Technol., 249 (2018) 328–333.
[26] F. Kazemi, H. Younesi, A. Asghar, N. Bahramifar, A. Heidari, Thiol-incorporated activated carbon derived from fir wood sawdust as an efficient adsorbent for the removal of mercury ion: batch and fixed-bed column studies, Process Saf. Environ. Prot., 100 (2015) 22–35.
[27] I.A. Aguayo-Villarreal, V. Hernández-Montoya, E.M. Ramírez-López, A. Bonilla-Petriciolet, M.A. Montes-Morán, Effect of surface chemistry of carbons from pine sawdust for the adsorption of acid, basic and reactive dyes and their bioregeneration using *Pseudomona putida*, Ecol. Eng., 95 (2016) 112–118.
[28] D. Božić, M. Gorgievski, V. Stanković, N. Štrbac, S. Šerbula, N. Petrović, Adsorption of heavy metal ions by beech sawdust - kinetics, mechanism and equilibrium of the process, Ecol. Eng., 58 (2013) 202–206.
[29] P.S. Thue, G.S. dos Reis, E.C. Lima, J.M. Sieliechi, G.L. Dotto, A.G.N. Wamba, S.L.P. Dias, F.A. Pavan, Activated carbon obtained from sapelli wood sawdust by microwave heating for o-cresol adsorption, Res. Chem. Intermed., 43 (2017) 1063–1087.
[30] E. Altıntıg, H. Altundag, M. Tuzen, A. Sarı, Effective removal of methylene blue from aqueous solutions using magnetic loaded activated carbon as novel adsorbent, Chem. Eng. Res. Des., 122 (2017) 151–163.
[31] H.N. Tran, S.J. You, H.P. Chao, Fast and efficient adsorption of methylene green 5 on activated carbon prepared from new chemical activation method, J. Environ. Manage., 188 (2017) 322–336.
[32] S. Hassan, A. Zahir, A. Khan, S. Afzal, M. Mansha, Adsorption of Mordant Red 73 dye on acid activated bentonite: kinetics and thermodynamic study, J. Mol. Liq., 254 (2018) 398–405.
[33] A. Khasri, O.S. Bello, M.A. Ahmad, Mesoporous activated carbon from Pentace species sawdust via microwave-induced KOH activation: optimization and methylene blue adsorption, Res. Chem. Intermed., 44 (2018) 5737–5757.
[34] H. Kalavathy, B. Karthik, L.R. Miranda, Removal and recovery of Ni and Zn from aqueous solution using activated carbon from *Hevea brasiliensis*: batch and column studies, Colloids Surf, B, 78 (2010) 291–302.
[35] Z. Heidarinejad, O. Rahmanian, M. Fazlzadeh, M. Heidari, Enhancement of methylene blue adsorption onto activated carbon prepared from Date Press Cake by low frequency ultrasound, J. Mol. Liq., 264 (2018) 591–599.
[36] M.V. Subbaiah, D.S. Kim, Adsorption of methyl orange from aqueous solution by aminated pumpkin seed powder: kinetics, isotherms, and thermodynamic studies, Ecotoxicol. Environ. Saf., 128 (2016) 109–117.
[37] S. Mohebali, D. Bastani, H. Shayesteh, Equilibrium, kinetic and thermodynamic studies of a low-cost biosorbent for the removal of Congo red dye: acid and CTAB-acid modified celery (*Apium graveolens*), J. Mol. Struct., 1176 (2019) 181–193.
[38] H.A. Ahsaine, M. Zbair, Z. Anfar, Y. Naciri, R. El haouti, N. El Alem, M. Ezahri, Cationic dyes adsorption onto high surface area 'almond shell' activated carbon: kinetics, equilibrium isotherms and surface statistical modeling, Mater. Today Chem., 8 (2018) 121–132.
[39] M. Andrea, E. De Franco, C.B. De Carvalho, M.M. Bonetto, R.D.P. Soares, L.A. Féris, Removal of amoxicillin from water by adsorption onto activated carbon in batch process and fixed bed column: kinetics, isotherms, experimental design and break-through curves modelling, J. Cleaner Prod., 161 (2017) 947–956.
[40] J.R. García, U. Sedran, M.A.A. Zaini, Z.A. Zakaria, Preparation, characterization, and dye removal study of activated carbon prepared from palm kernel shell, Environ. Sci. Pollut. Res., 25 (2018) 5076–5085.
[41] V. Tharaneedhar, P. Senthil Kumar, A. Saravanan, C. Ravikumar, V. Jaikumar, Prediction and interpretation of adsorption parameters for the sequestration of methylene blue dye from aqueous solution using microwave assisted corncob activated carbon, Sustainable Mater. Technol., 11 (2017) 1–11.
[42] M.J. Ahmed, Potential of *Arundo donax* L. stems as renewable precursors for activated carbons and utilization for wastewater treatments: review, J. Taiwan Inst. Chem. Eng., 63 (2016) 336–343.
[43] M.S. Monteiro, R.F. de Farias, J.A.P. Chaves, S.A. Santana, H.A.S. Silva, C.W.B. Bezerra, Wood (*Bagassa guianensis Aubl*) and green coconut mesocarp (*cocos nucifera*) residues as textile dye removers (Remazol Red and Remazol Brilliant Violet), J. Environ. Manage., 204 (2017) 23–30.
[44] O.S. Bello, T.T. Siang, M.A. Ahmad, Adsorption of Remazol Brilliant Violet-5R reactive dye from aqueous solution by cocoa pod husk-based activated carbon: kinetic, equilibrium and thermodynamic studies, Asia-Pacific J. Chem. Eng., 7 (2012) 378–388.
[45] A. Kumar, H.M. Jena, Removal of methylene blue and phenol onto prepared activated carbon from Fox nutshell by chemical activation in batch and fixed-bed column, J. Cleaner Prod., 137 (2016) 1246–1259.
[46] L. Wang, Z. Chen, H. Wen, Z. Cai, C. He, Z. Wang, W. Yan, Microwave assisted modi fi cation of activated carbons by organic acid ammoniums activation for enhanced adsorption of acid red 18, Powder Technol., 323 (2018) 230–237.
[47] K.M. Doke, E.M. Khan, Equilibrium, kinetic and diffusion mechanism of Cr(VI) adsorption onto activated carbon derived from wood apple shell, Arab. J. Chem., 10 (2017) S252–S260.
[48] S.N. Jain, P.R. Gogate, Adsorptive removal of acid violet 17 dye from wastewater using biosorbent obtained from NaOH and H_2SO_4 activation of fallen leaves of *Ficus racemosa*, J. Mol. Liq., 243 (2017) 132–143.
[49] C. Ribeiro, D. Sérgio, A. Silva, C. Carvalho, A.P. Vieira, C. Wellington, B. Bezerra, Removal of Remazol brilliant violet textile dye by adsorption using rice hulls, Polímeros, 27 (2017) 16–26.
[50] A. Khasri, M.A. Ahmad, Adsorption of basic and reactive dyes from aqueous solution onto Intsia bijuga sawdust-based activated carbon: batch and column study, Environ. Sci. Pollut. Res., 25 (2018) 31508–31519.